


3-2014

Numerical Analysis of First-order Acousto-optic Bragg Diffraction of Profiled Optical Beams using Open-loop Transfer Functions

Monish Ranjan Chatterjee
University of Dayton, mchatterjee1@udayton.edu

Fares S. Almeahmadi
University of Dayton

Follow this and additional works at: https://ecommons.udayton.edu/ece_fac_pub

 Part of the [Computer Engineering Commons](#), [Electrical and Electronics Commons](#), [Electromagnetics and Photonics Commons](#), [Optics Commons](#), [Other Electrical and Computer Engineering Commons](#), and the [Systems and Communications Commons](#)

eCommons Citation

Chatterjee, Monish Ranjan and Almeahmadi, Fares S., "Numerical Analysis of First-order Acousto-optic Bragg Diffraction of Profiled Optical Beams using Open-loop Transfer Functions" (2014). *Electrical and Computer Engineering Faculty Publications*. 332.
https://ecommons.udayton.edu/ece_fac_pub/332

This Article is brought to you for free and open access by the Department of Electrical and Computer Engineering at eCommons. It has been accepted for inclusion in Electrical and Computer Engineering Faculty Publications by an authorized administrator of eCommons. For more information, please contact frice1@udayton.edu, mschlangen1@udayton.edu.

Optical Engineering

SPIDigitalLibrary.org/oe

Numerical analysis of first-order acousto-optic Bragg diffraction of profiled optical beams using open- loop transfer functions

Monish R. Chatterjee
Fares S. Almealmadi

Numerical analysis of first-order acousto-optic Bragg diffraction of profiled optical beams using open-loop transfer functions

Monish R. Chatterjee* and Fares S. Almeahmadi

University of Dayton, Department of Electrical and Computer Engineering, 300 College Park, Dayton, Ohio 45469

Abstract. In standard acousto-optic Bragg analysis, the incident light and sound beams are assumed to be uniform plane waves (with constant profiles) leading to the results based on standard weak interaction theory. As a follow-up to earlier work dealing with nonuniform incident optical beams, we revisit the problem of Bragg diffraction under nonuniform profiles, and include Gaussian, third-order Hermite–Gaussian, and zeroth-order Bessel profiles in our investigation, along with a few others. The first-order diffracted beam is examined (using a transfer function formalism based on angular spectra) under several parametric limits [such as the Klein–Cook parameter Q , the effective profile width, and the optical phase-shift parameter ($\hat{\alpha}_0$) in the sound cell]. Wherever feasible, the numerical results are compared with analytic theory. The scattered first-order profile output versus the optical phase-shift appears to maintain behavior similar to the known first-order characteristics (\sin^2 in intensity) encountered for the uniform incident beam case. It is observed, however, that such conformity exists seemingly only at relatively small values of Q (typically about 20 to 50). At higher Q s, on the other hand (where one would otherwise expect behavior closer to standard Bragg theory based on large Q s), it is found that the first-order intensity deviates substantially from the expected \sin^2 - (or related) pattern. This deviation actually becomes more severe at even higher Q s. Additionally, the output profiles at higher Q s are also found to be distorted relative to the incident profiles. These results, though anomalous, are nevertheless generally compatible with earlier studies. Based on the transfer function theory, it is also known that for very large optical phase shifts (i.e., when $\hat{\alpha}_0$ goes to infinity), the scattered first-order output for a Gaussian profile undergoes an axial (spatial) shift past the output plane of the sound cell. This predicted result is corroborated in our numerical simulation for both the Gaussian and third-order Hermite–Gaussian profiles, but not the zeroth-order Bessel or Airy profiles. These results provide both confirmation of some expected behavior for profiled beam scattering (including likely affirmation of the well known and unique diffractionless properties of certain Bessel beams), but also some insight into unexpected and anomalous photon-phonon interaction behavior. © 2014 Society of Photo-Optical Instrumentation Engineers (SPIE) [DOI: 10.1117/1.OE.53.3.036108]

Keywords: acousto-optics; Bragg regime; photon; phonon; profiled beams; Gaussian; Hermite–Gaussian; Bessel; Klein–Cook parameter; optical phase shift; angular spectra; transfer function; scattered profiles; diffractionless beams.

Paper 131618P received Oct. 24, 2013; revised manuscript received Jan. 27, 2014; accepted for publication Mar. 4, 2014; published online Mar. 27, 2014.

1 Introduction

The phenomenon of acousto-optic (A-O) diffraction, first studied extensively in the late 1920s and 1930s,^{1,2} is used in many areas of signal processing. Although this behavior is complex and despite extensive generalized analyses, comprehension of the phenomenon in its entirety is still incomplete.³ A-O diffraction refers to the interaction of light and sound waves, and it is used to controllably diffract light beams. The behavior of an A-O cell depends on several system parameters, and in particular, the thickness of the crystal L and the wave numbers of both sound (K) and light (k). These quantities are summarized as a figure-of-merit by the Klein–Cook parameter (Q) which is used to characterize the regimes of A-O operation.⁴ For strict Bragg operation, which finds the most applications for these devices in practice, Chen and Chatterjee showed that Q should be larger than 8π .⁵ In this regime, under perfect Bragg-matching, there is only one diffracted order. If Q is much smaller than one, the mode of operation is called the Raman–Nath regime,

which is characterized by multiple diffracted orders with the intensities given by Bessel functions.^{6,7}

Weak interaction theory is used in the analyses of AO diffraction, and this theory rests upon the assumption of uniform plane waves of sound and light. These assumptions, though not physically realistic, allow for tractable analyses and lead to observable results. In 1979, a plane wave theory of A-O interaction was developed by Korpel and Poon, in which the light and sound waves are represented by plane wave decomposition.⁷ This theory (for uniform light and profiled sound) leads to well-known expressions for Bragg and Raman–Nath diffraction. However, there is much that is unknown about A-O diffraction with profiled beams, which are physically more realistic. Extensive research has been conducted to analyze special cases such as two-dimensional (2-D) and three-dimensional (3-D) sound profiles, and higher-order or strong interactions.^{8,9} Nevertheless, examining A-O scattering under arbitrary beam profiles remains a complex problem. Beginning with the multiple plane wave theory due to Korpel and Poon,⁷ Chatterjee et al. obtained

*Address all correspondence to: Monish R. Chatterjee, E-mail: mchatterjee1@udayton.edu

a transfer function formalism for evaluating scattered output profiles for arbitrary input profiles.¹⁰ The results of that approach under the current series of examinations have been found to be occasionally counter-intuitive, as will be shown.

The transfer function approach utilizes a plane wave angular spectrum of the field distribution (valid for small deviations from the exact Bragg angle), which allows the scattered fields to be represented by Fourier integrals in the angular domain. This makes it possible to apply the Fast Fourier Transform (FFT) to numerically generate the scattered fields of arbitrary inputs. Transfer function expressions for both Bragg orders are developed and may be readily applied in the Fourier transform domain. These expressions are convenient for modeling the effects of various parameters (such as phase shift and Q), as well as arbitrary input profiles. It was shown earlier that under the asymptotic limit of high (peak) phase shift, there should occur an axial shift of the output scattered profile for Gaussian input optical profiles.¹⁰

The current work was motivated by recent investigations involving AC signal modulation and encryption using chaos in hybrid A-O feedback systems.^{11,12} Although these investigations clearly demonstrated the feasibility of encrypting, transmitting, and recovering relatively low-bandwidth AC signals (up to about 1 MHz), they were essentially based on the assumption of uniform optical and acoustic beams. Since practical optical beams are more likely to be nonuniform in profile, and chaos is extremely sensitive to amplitudes, it becomes necessary to examine the consequences of specific profiled light beams upon the feedback system under examination. To acquire a closer insight into the scattering properties of the Bragg cell under profiled beam propagation, the system has been initially studied strictly in open-loop. The current paper is primarily a report on the findings relative to this open-loop problem. To this end, the transfer function formalism is applied to evaluate the first-order scattered outputs using a variety of input profiles, including Gaussian, third-order Hermite–Gaussian, and zeroth-order Bessel beams. In examining the asymptotic axial behavior due to the zeroth-order Bessel beam, it was discovered that such a beam produces relatively negligible axial shifts. This has prompted further investigations of Airy-type and non-Airy-type beams in order to ascertain if there is any underlying common physical property inherent to such observations. These findings are also reported here.

With each of these profiles, the behavior of the scattered light is thoroughly explored as a function of various parameters. We examine the first-order output profiles under three different values of the Klein–Cook parameter, different widths of the input beam profiles, and several values of the sound pressure (i.e., the peak optical phase shift through the sound cell). The first-order scattered output is examined along both the (normalized) transverse radial coordinate and as a function of the optical phase shift. Nominally, one would expect the scattered output profiles to be very different from that predicted by standard uniform profile theory. Additionally, the scattered profiles will likely depend on the system parameters such as Q and $\hat{\alpha}_0$. Such a behavior, if present, will impact the closed-loop characteristics of the hybrid feedback system mentioned earlier.^{13,14}

The transfer function formalism for arbitrary input beams is first introduced in Sec. 2, along the lines of the original

development by Chatterjee et al.¹⁰ The numerical simulation of the transfer function formalism begins with a Gaussian incident profile, as described in Sec. 3.1. Third-order Hermite–Gaussian and zeroth-order Bessel profiles are presented in Secs. 3.2 and 3.3, respectively. In Sec. 3.4, the asymptotic limit of the first-order beam profile as $\hat{\alpha}_0 \rightarrow \infty$ is discussed for five different optical beams, wherein we have also included the Airy disk profile and the $J_2(x)/x$ beam. The numerical results generated by these five cases are analyzed and interpreted in Sec. 4. Section 5 provides concluding remarks along with future work involving the closed-loop system and its various nonlinear dynamical domains. Some results from the latter work are in process for publication elsewhere.

2 Transfer Function Formalism (TFF) for Arbitrary Input Optical Profiles

Figure 1 illustrates the standard geometry of an A-O Bragg cell, showing two scattered orders created by an arbitrary input profile, assuming upshifted operation at the (exact) Bragg incidence. We assume that the profiled beam is nominally incident at the Bragg angle [i.e., the “ray” (or wave vector) corresponding to the center of the profiled beam is incident at the Bragg angle]. In this figure, r and r' represent the transverse radial coordinates with respect to the direction of the incident field and the diffracted field, respectively. $E_0(r)$ and $E_1(r')$ represent the zeroth-order and first-order scattered outputs, δ is a dimensionless measure of the angular deviation from the nominal Bragg angle $\phi_B (\approx K/2k)$, and \bar{K} is the acoustic wave vector.¹⁰

Both diffracted orders can be described by a set of coupled differential equations given by⁷

$$\frac{d\tilde{E}_n}{d\xi} = -j \left(\frac{\hat{\alpha}}{2} \right) \left(e^{\left\{ -j \left(\frac{\delta}{2} \right) \left[\frac{\phi_{\text{inc}}}{\phi_B} + (2n-1) \right] Q \xi \right\}} \tilde{E}_{n-1} + e^{\left\{ j \left(\frac{\delta}{2} \right) \left[\frac{\phi_{\text{inc}}}{\phi_B} + (2n+1) \right] Q \xi \right\}} \tilde{E}_{n+1} \right). \quad (1)$$

In this equation, $\hat{\alpha} (= kC|A|L/2)$ is the peak phase delay, $\xi (= z/L)$ is the normalized propagation distance in the sound cell, ϕ_{inc} is the incident angle corresponding to a uniform plane wave input, ϕ_B is the Bragg angle of the sound cell, and Q is the Klein–Cook parameter.¹⁰ This general equation leads to the two scattered orders \tilde{E}_0 and \tilde{E}_1 for near-Bragg diffraction by setting $\phi_{\text{inc}} [= -(1 + \delta)\phi_B]$. With this substitution for

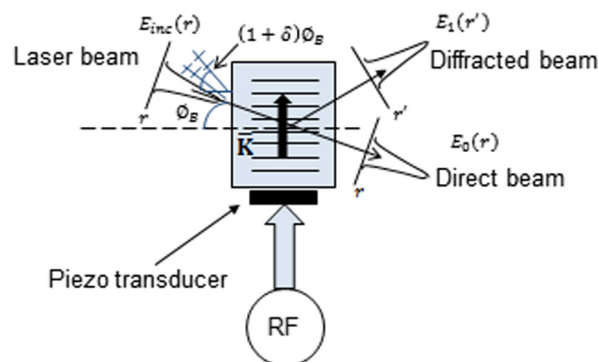


Fig. 1 Bragg diffraction with an arbitrary incident beam profile.

near-Bragg incidence with an angular deviation factor δ , the coupled equations reduce to the following:

$$\frac{d\tilde{E}_0}{d\xi} = -j\left(\frac{\hat{\alpha}}{2}\right)e^{-jQ\xi\delta/2}\tilde{E}_1, \quad (2)$$

$$\frac{d\tilde{E}_1}{d\xi} = -j\left(\frac{\hat{\alpha}}{2}\right)e^{jQ\xi\delta/2}\tilde{E}_0. \quad (3)$$

The transfer function formalism due to Chatterjee et al.¹⁰ is a direct consequence of the solutions of the above coupled equations. As may be shown, the solutions for the zeroth- and first-orders under arbitrary angular deviations from the Bragg angle, when normalized relative to the incident beam angular spectrum, yield the following two transfer functions for the fields in the δ domain. Thus we have¹⁰

$$\begin{aligned} \tilde{H}_0(\delta) &= \frac{\tilde{E}_0(\xi)_{\xi=1}}{\tilde{E}_{\text{inc}}} \\ &= -\frac{e^{-j\frac{\delta Q}{4}}}{\sqrt{\left(\frac{\delta Q}{4}\right)^2 + \left(\frac{\hat{\alpha}}{2}\right)^2}} \left\{ \sqrt{\left(\frac{\delta Q}{4}\right)^2 + \left(\frac{\hat{\alpha}}{2}\right)^2} \right. \\ &\quad \times \cos \left[\sqrt{\left(\frac{\delta Q}{4}\right)^2 + \left(\frac{\hat{\alpha}}{2}\right)^2} \right] \\ &\quad \left. + j\frac{\delta Q}{4} \sin \left[\sqrt{\left(\frac{\delta Q}{4}\right)^2 + \left(\frac{\hat{\alpha}}{2}\right)^2} \right] \right\}, \quad (4) \end{aligned}$$

$$\begin{aligned} \tilde{H}_1(\delta) &= \frac{\tilde{E}_1(\xi)_{\xi=1}}{\tilde{E}_{\text{inc}}} \\ &= -j\left(\frac{\hat{\alpha}}{2}\right) \frac{e^{j\frac{\delta Q}{4}}}{\sqrt{\left(\frac{\delta Q}{4}\right)^2 + \left(\frac{\hat{\alpha}}{2}\right)^2}} \left\{ \sin \left[\sqrt{\left(\frac{\delta Q}{4}\right)^2 + \left(\frac{\hat{\alpha}}{2}\right)^2} \right] \right\}. \quad (5) \end{aligned}$$

Incidentally, we note here that in the late 1970s Magdich and Molchanov analyzed the problem of the diffraction of a general optical beam by strong acoustic waves at length in a series of papers (see, for instance, Refs. 15–17). It turns out that the input beams considered by them included both profiled plane waves as well as curved wavefronts. The formalism developed by Chatterjee et al., on the other hand, considers primarily profiled plane waves of light subjected to sound waves of variable intensity. The emphasis in the above formalism is the development of an equivalent transfer function for the zeroth- and first-orders, whereby the spatial output profiles may be evaluated through Fourier inversion of the output spectrum. Incidentally, these transfer functions, with minor modifications, have been used in interesting applications such as one-dimensional and 2-D edge detection of images using multiple Bragg cells.^{18,19} However, the derivation in Ref. 16 indicates that the diffracted (first-order) light distribution expressed as a product of the far-field incident light profile and a distribution due to the light-sound interaction in the Bragg cell (via the a and b parameters in Ref. 16) is similar to $\tilde{E}_0(\xi)$ and $\tilde{E}_1(\xi)$ in Eqs. (4) and (5) above. Hence, the transfer functions defined above may

be considered equivalent to the distribution functions described in Ref. 16.

Both scattered beams may now be found by applying an inverse Fourier transform to the product of the incident spectrum and the corresponding transfer function, $\tilde{E}_{\text{inc}}(\delta)H(\delta)$.¹⁰ This process is shown in the following equation, where $E_{\text{out}}(r)$ is either first-order or zeroth-order output, depending on the transfer function used, and $\tilde{E}_{\text{inc}}(\delta)$ is the angular spectrum of the incident profiled beam

$$E_{\text{out}}(r) = \int_{-\infty}^{\infty} \tilde{E}_{\text{inc}}(\delta)H(\delta)e^{-j\frac{2\pi}{\lambda}\delta\phi_B r} \left(\frac{\phi_B}{\lambda}\right) d\delta. \quad (6)$$

In the results reported below, the angular spectrum of the incident light is inserted into this equation, and the output fields are computed by numerically solving the same. These fields are functions of the peak phase delay $\hat{\alpha}_0$ and the Klein–Cook parameter Q . Three different incident profiles $E_{\text{inc}}(r)$ are tested for determining the output profile characteristics: viz., the Gaussian, third-order Hermite–Gaussian, and zeroth-order Bessel profiles.

3 Numerical Results

In this section, numerical results for the first-order scattered output for each of three incident optical beams are illustrated graphically. Low and high values of the Klein–Cook parameter are tested in each case. Additionally, a uniform input is approximated using a wide Gaussian beam in order to verify that the spectral simulation will produce the well-known results for uniform plane wave inputs. Also, high sound pressure is applied to simulate the asymptotic spatial shift of the output. The following three sections present the simulation results separately for the three input profiles, and the fourth section presents the asymptotic shift results for all profiles.

3.1 Output Profiles for a Gaussian Incident Beam Using TFF

The absolute value of the scattered first-order output beam $|E_1(r', \hat{\alpha})|$ with a Gaussian incident profile is shown in Fig. 2 for $Q = 20$. The 3-D plot shown in Fig. 2 indicates

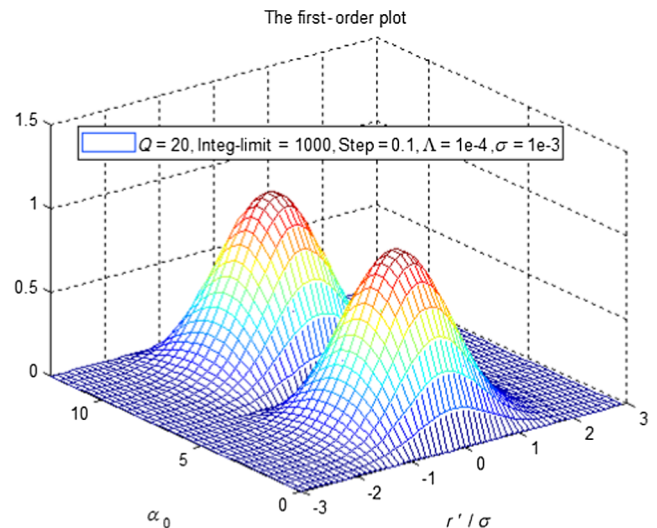


Fig. 2 Scattered first-order beam output with a Gaussian incident beam profile for $Q = 20$.

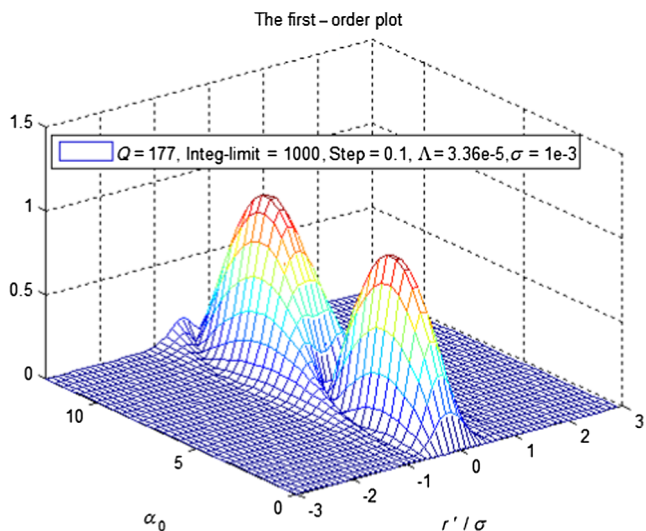


Fig. 3 Scattered first-order beam output with a Gaussian incident beam profile for $Q = 177$.

that the plot appears to maintain behavior similar to that for uniform plane wave in the $\hat{\alpha}_0$ direction, even though it appears to have a Gaussian profile. The cross section through Fig. 2 along the peak phase shift dimension $\hat{\alpha}_0$ has the appearance of a sinusoid, which is reminiscent of uniform plane wave behavior. Along the normalized transverse radial coordinate for $\hat{\alpha}_0 = \pi$, the cross section is approximately Gaussian, thereby verifying the expected result for relatively low Q s.

When Q is increased to 177 (note that doing this requires an adjustment of the sound wavelength), we obtain the result shown in Fig. 3, which illustrates the first-order beam output $|E_1(r', \hat{\alpha})|$ along both the peak phase shift dimension $\hat{\alpha}_0$ and the normalized transverse radial coordinate. The 3-D plot shown in Fig. 3, however, shows behavior different from the low- Q case. Thus, as evident from the cross section through Fig. 3, the first-order along the peak phase shift dimension $\hat{\alpha}_0$ is no longer sinusoidal, thereby diverging from the uniform result. Likewise, the cross section along the normalized transverse radial coordinate for $\hat{\alpha}_0 = \pi$ no longer exhibits Gaussian profile, with small sidelobes clearly visible.

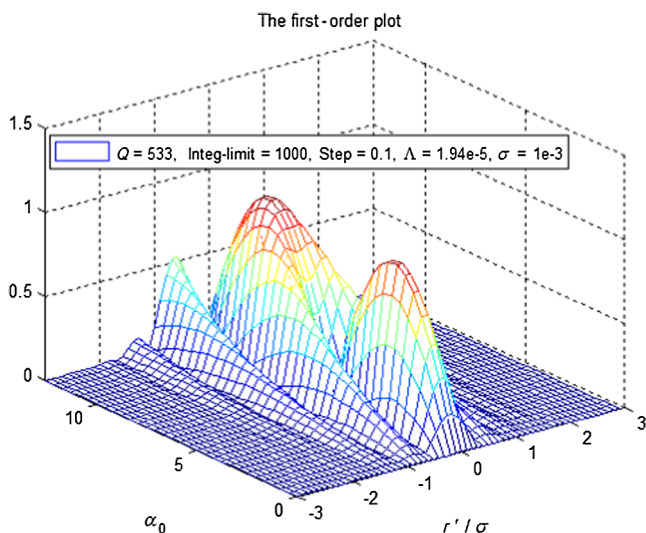


Fig. 4 Scattered first-order beam output with a Gaussian incident beam profile for $Q = 533$.

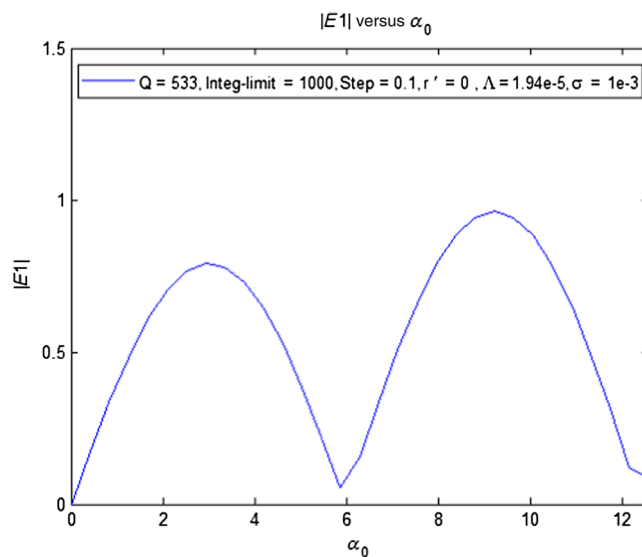


Fig. 5 First-order Bragg diffraction versus the optical phase shift (cross section from Fig. 4).

As a special note, we observe the following relative to the choice of the high value (533) of Q chosen here. First, this choice (as well as those of $Q = 20$ and 177) is prompted by the desire to draw direct comparisons with results previously presented in Ref. 10. However, it turns out that requiring a very high Q , especially in an experimental setup, may lead to reduced diffraction efficiency and device bandwidth. Our purpose in pursuing this high Q value, however, is very different. Our ultimate aim is to study the effect of profiled optical beams propagating through A-O Bragg cells with different Q s under positive electronic feedback of the first-order output. The generation and application of resulting chaos in such a device have been studied recently at some length for uniform plane waves of light. From this perspective, any reduction in the device efficiency or BW, while a drawback, is relatively unimportant for the purpose of this paper. Hence, when Q is increased to 533, additional deviations are observed, as shown in Figs. 4–6. These plots

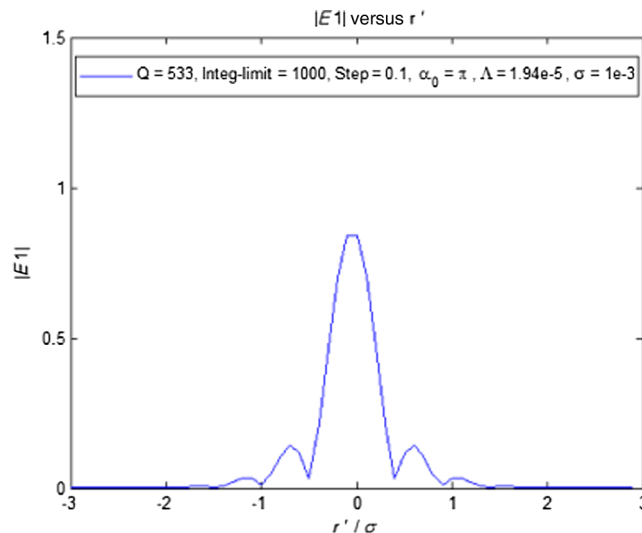


Fig. 6 First-order Bragg diffraction versus the normalized transverse radial coordinate (cross section from Fig. 4).

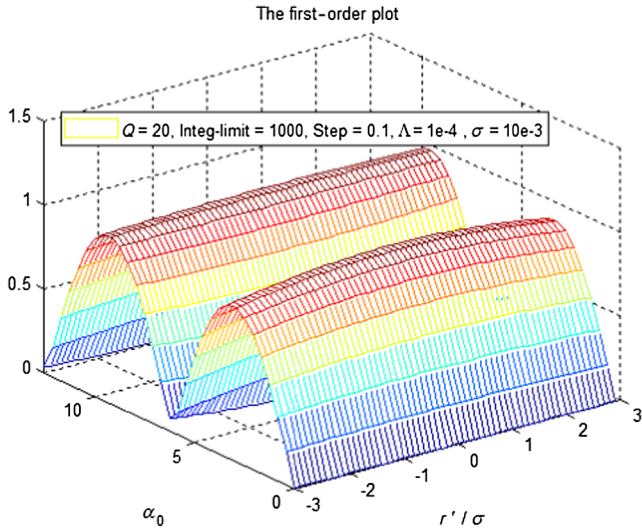


Fig. 7 Scattered first-order beam output with a very wide Gaussian incident beam.

illustrate the absolute value of the scattered first-order beam output $|E_1(r', \hat{\alpha})|$ from the same three perspectives. Figure 4 shows the 3-D behavior and Fig. 5 illustrates the output cross section along the peak phase shift dimension $\hat{\alpha}_0$, as may be seen from Fig. 7, shows the expected. We find that the output is further distorted relative to the usual sinusoidal $\hat{\alpha}_0$ profile for the uniform case. Similarly, Fig. 6 shows further deviation from the Gaussian shape of the cross section along the normalized transverse radial coordinate for $\hat{\alpha}_0 = \pi$.

In order to compare the above results with those for a uniform plane wave input profile, a very wide Gaussian input was simulated for $Q = 20$. This result, with the Gaussian 10 times wider, is shown in 3-D in Fig. 7 and is consistent with well-known results. The output cross section along the peak phase shift dimension $\hat{\alpha}_0$ is showing the expected sinusoidal behavior. The cross section along the normalized transverse radial coordinate for $\hat{\alpha}_0 = \pi$, as shown in Fig. 8, is nearly uniform. This result affirms the validity of the integral formalism.

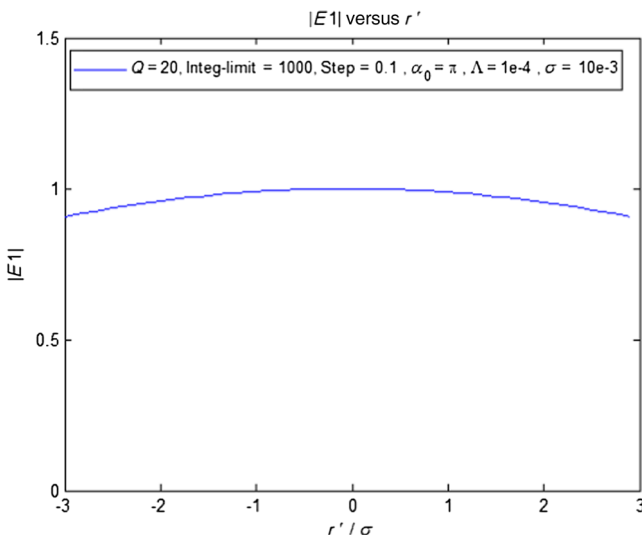


Fig. 8 First-order Bragg diffraction versus the normalized transverse radial coordinate (cross section from Fig. 7).

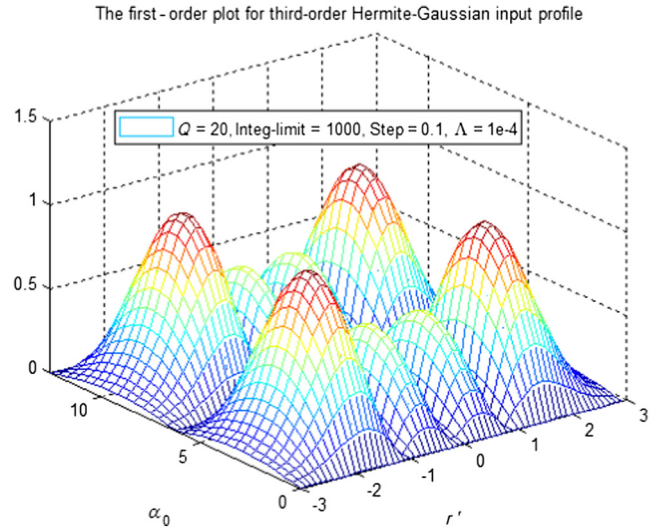


Fig. 9 Scattered first-order beam output with a third-order Hermite-Gaussian incident beam profile for $Q = 20$.

3.2 Output Profiles for a Third-Order Hermite-Gaussian Incident Beam Using TFF

The scattered first-order output beam $|E_1(r', \hat{\alpha})|$ with a third-order Hermite-Gaussian incident profile is shown in Fig. 9 for $Q = 20$. The 3-D plot is shown in Fig. 9, and for this relatively low Q , this plot maintains the expected behavior to the extent that the output maintains its profile shape. The cross section through Fig. 9 along the peak phase shift dimension $\hat{\alpha}_0$ again has the appearance of a sinusoid. Figure 10 shows the cross section along the normalized transverse radial coordinate for $\hat{\alpha}_0 = \pi$, and it approximates the shape of a third-order Hermite-Gaussian. The simulation results for higher Q s (not shown here), are distorted along both dimensions, as was seen with the Gaussian inputs.

3.3 Output Profiles for a Zeroth-Order Bessel Incident Beam Using TFF

The scattered first-order output beam $|E_1(r', \hat{\alpha})|$ with a zeroth-order Bessel incident profile is shown in Fig. 11 for

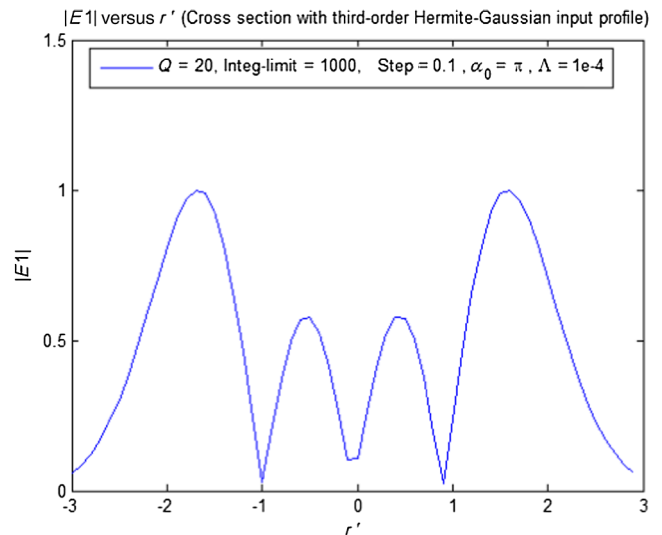


Fig. 10 First-order Bragg diffraction versus the transverse radial coordinate (cross section from Fig. 9).

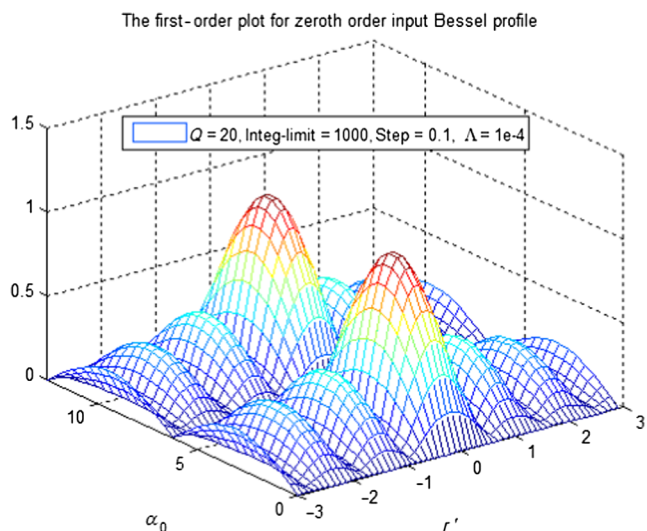


Fig. 11 Scattered first-order beam output with a Bessel incident beam profile for $Q = 20$.

$Q = 20$. The 3-D plot shown in Fig. 11 for this low Q appears to follow the expected behavior with the output maintaining its profile shape. The cross section through Fig. 11 along the peak phase shift dimension $\hat{\alpha}_0$ has the appearance of a sinusoid. Figure 12 shows the cross section along the normalized transverse radial coordinate for $\hat{\alpha}_0 = \pi$, and it approximates the shape of a zeroth-order Bessel function. The simulation results for higher Q s, which are not shown here, are only slightly distorted along both dimensions, unlike the other two previous cases.

3.4 Asymptotic Limit of the First-Order Diffracted Profile

For high sound pressure (i.e., large $\hat{\alpha}_0$), a spatial shift in the output profile for Gaussian input profiles is predicted by the spectral theory in Ref. 10. As $\hat{\alpha}_0$ goes to infinity, this theory predicts an asymptotic shift off center spatially

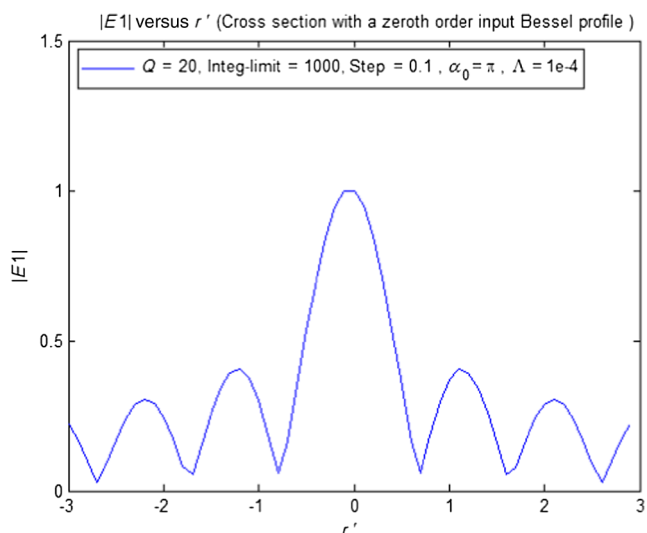


Fig. 12 First-order Bragg diffraction versus the transverse radial coordinate (cross section from Fig. 11).

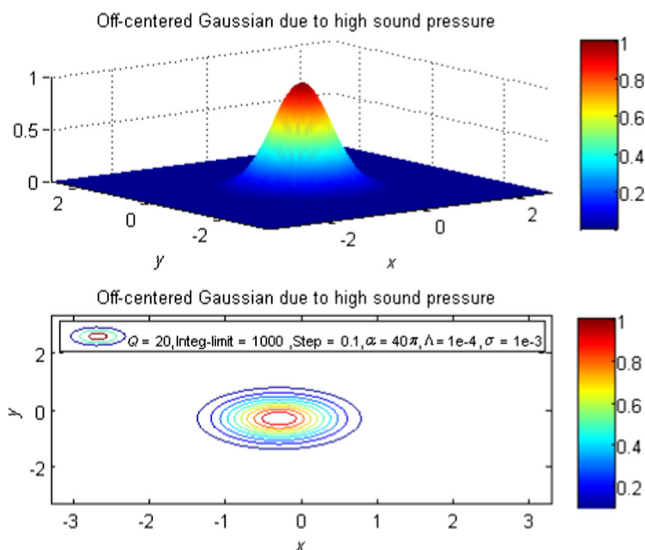


Fig. 13 Asymptotic axial shift of the Gaussian beam center as predicted by the transfer function formalism.

to $-Q\Lambda/4\pi$. The shift to a negative r' is somewhat puzzling, and may be resolved by studying the numerical plot. The previous simulations (at low sound pressures) show negligible shift. The simulation results for high sound pressure are shown in Figs. 13–15 for the Gaussian, third-order Hermite–Gaussian, and zeroth-order Bessel profiles, respectively. The contour lines in Fig. 13 clearly illustrate the shifted center for a Gaussian beam, using $\hat{\alpha}_0 = 40\pi$. Similarly, the contour lines in Fig. 14 illustrate a discernible shift for a third-order Hermite–Gaussian. The shift off-center for both cases occurs only to one side of the radial axis. However, it is observed that there is negligible shift off-center for a Bessel profile, as shown by the contour lines in Fig. 15. This result, though analytically unanticipated, appears to affirm the diffractionless property of certain Bessel beams.^{20,21}

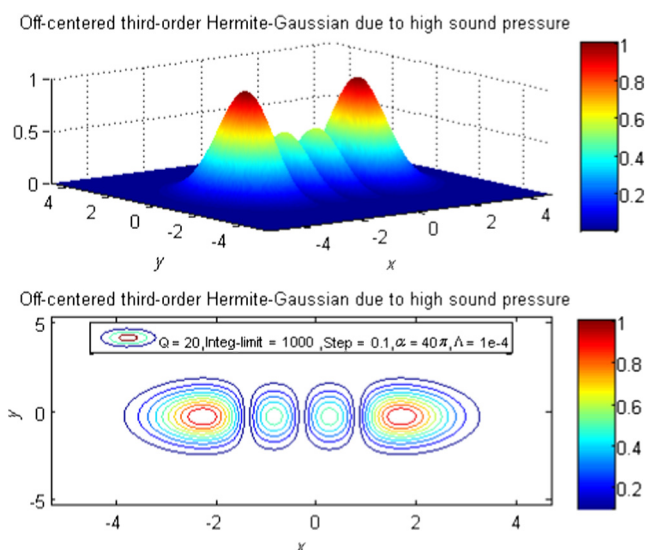


Fig. 14 Asymptotic axial shift of the third-order Hermite–Gaussian beam center as predicted by the TFF.

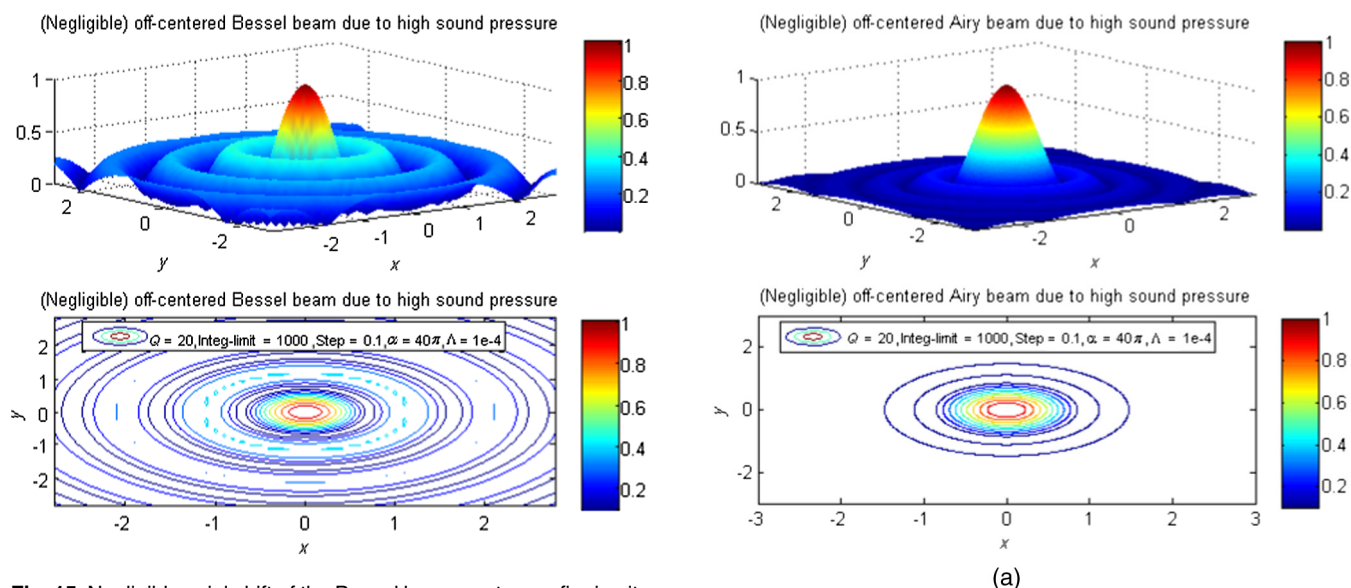


Fig. 15 Negligible axial shift of the Bessel beam center confirming its unique diffractionless property.

4 Interpretation and Analysis of Profiled Beam Numerical Results

To compare the simulations of diffracted outputs via inverse angular spectra to known results for diffraction of uniform profile, a uniform plane wave input was visualized as the limit of a very broad Gaussian. We note that this result may also be derived by directly incorporating a uniform plane wave profile into the diffraction formalism. This result is presented in Appendix A. As seen from Fig. 7, the simulation results match known plane wave output behavior, viz., sinusoidal dependence on $\hat{\alpha}_0$, and approximately uniform in profile along r' . Another observation for a variety of input profiles is that the scattered output versus $\hat{\alpha}_0$ continues to maintain a sinusoidal shape at relatively low values of Q (about 20 to 50 or 6π to 16π). At higher Q values (such as 177 and 533 as presented here), however, the shape of the first-order versus $\hat{\alpha}_0$ begins to distort somewhat in amplitude, even if maintaining a rectified sinusoidal shape. These results are counter-intuitive since at higher Q values, an A-O cell is expected to behave closer to ideal Bragg diffraction than for lower Q s. Clearly, at higher Q s, a profiled, nonuniform input beam does not emerge as $\sin(\hat{\alpha}_0/2)$ unlike the case for a uniform profile; for lower Q s (higher than 2π), however, it maintains a sinusoidal shape. The case for a zeroth-order Bessel beam ($J_0(x)/x$) profile presents an interesting observation. We remark here that the asymptotic radial profiles for Gaussian and Hermite–Gaussian inputs show an axial shift of the center of the scattered beam, as predicted by theory for large $\hat{\alpha}_0$ (shown in Figs. 13 and 14). On the other hand, that for a zeroth-order Bessel beam shows virtually no shift at all. This result appears to affirm the diffractionless property of a zeroth-order or certain other Bessel beams.^{20,21} To verify this feature further, we also tested the integral formalism for an Airy beam (of the kind $J_1(x)/x$ in amplitude) and a second-order Bessel beam, $J_2(x)/x$. The results show that the Airy beam tends to remain undiffracted at large $\hat{\alpha}_0$, while the $J_2(x)/x$ beam exhibits axial shifts like the Gaussian. These results are shown in Figs. 16(a) and 16(b). Overall, the axial shift investigations indicate that beam profiles with a central maximum accompanied by progressively decaying

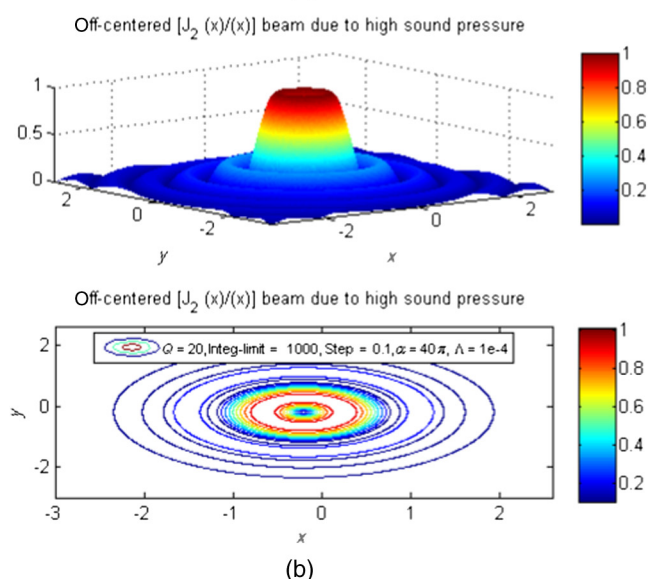


Fig. 16 (a) Negligible axial shift of the Airy beam center confirming its unique diffractionless property. (b) The axial shift of the $J_2(x)/x$ beam center due to the high sound pressure.

positive and negative excursions [such as $J_0(x)$ and $J_1(x)/x$] will likely not undergo much axial diffraction or scattering, while all other beam profiles will. Overall, we observe that while these results are corroborated by the simulation results discussed here, and are in general conformity with known Bessel-beam (and other nondiffracting beams) properties, the mathematical formalism developed and discussed here does not provide any intuitive insight into this phenomenon *per se*. Suffice it to say that in the earlier treatment,¹⁰ this was mathematically shown to be so for the case of the Gaussian beam (which, while having a central maximum, nevertheless lacks positive and negative decaying sidelobes) as $\hat{\alpha}_0 \rightarrow \infty$, whereby it does suffer axial shifts in the asymptotic limit. The behavior of the simulated outputs is found to depend upon the range of the Klein–Cook parameter Q used in the simulation. For Q between 20 and 50, the shape of the output profile along the normalized radial coordinate is similar to the input profile for all profiles tested in the present work. Likewise, along the peak phase delay dimension, the output is

sinusoidal for all profiles tested. For higher values of Q (closer to exact Bragg behavior), one would expect the scattered output to more closely adhere to uniform plane wave input behavior. However, as seen in Figs. 3 and 4, the simulation generates unexpected results for a Gaussian input profile along both $\hat{\alpha}_0$ and r' , including amplitude distortions and secondary (side) lobes. In follow-up work (some of which is ongoing), the effects of such deviations on a hybrid feedback system analyzed in recent research with uniform plane waves for chaotic encryption applications,^{11,12} will be investigated in some detail.

5 Concluding Remarks

The standard analysis of Bragg cells begins with the assumption of uniform plane waves of sound and light input. This work, based on Bragg analysis of profiled optical beams and uniform sound waves, shows that the diffracted output exhibits extensive deviations from uniform plane wave behavior, thereby making it crucial to the analysis of closed-loop feedback systems that depend critically on the diffracted amplitudes for their nonlinear dynamics. To better understand the Bragg behavior for nonuniform inputs, this work applies a transfer function approach in order to simulate various profiled outputs. The first-order scattered output is generated by multiplying the input spectrum by a transfer function and numerically computing the inverse Fourier transform of the product. This process was tested by duplicating known results for uniform plane wave inputs, and by numerically producing the spatial shift that is predicted for infinitely high sound pressures. Interestingly, the shift off-center occurs only on one side of the radial axis (toward the third quadrant in the transverse plane), and explanation of such a phenomenon (using wave interference or photon-phonon interaction models) is pending. Unexpected deviations from the standard theory are observed for high Q values, effects likely to impact the performance of the A-O hybrid feedback system. The fact that these deviations are due to specific profiled incident beams is confirmed by the results for a zeroth-order and Airy Bessel beams, which are not significantly shifted or diffracted off-axis during diffraction at high $\hat{\alpha}_0$ values. These results indicate that beams with central peaks followed by decaying positive and negative excursions exhibit diffraction immunity. The results from this simulation will be applied next to study the impact of nonuniform profiled input beams on the closed-loop feedback behavior en route to bistability and chaos. The current work establishes the open-loop characteristics of the scattered first-order output and this will be numerically incorporated into a closed-loop system in order to examine the nonlinear dynamics of profiled beam propagation under feedback and thereby realize and derive new insights into encrypted signal transmission and recovery.

Appendix A

- i. First-order output corresponding to a uniform plane wave input

$$E_{\text{inc}}(r) = A \Rightarrow \tilde{E}_{\text{inc}}(\delta) = \frac{\lambda}{\phi_B} \int_{-\infty}^{\infty} E(r) e^{-j\frac{2\pi}{\lambda}\delta\phi_B r} dr$$

$$= A \left(\frac{\lambda}{\phi_B} \right) \delta_1(\delta), \tag{7}$$

where δ_1 is the unit impulse function. Hence, since

$$E_1(r') = \int_{-\infty}^{\infty} \tilde{E}_{\text{inc}}(\delta) H_1(\delta) e^{-j\frac{2\pi}{\lambda}\delta\phi_B r'} \left(\frac{\phi_B}{\lambda} \right) d\delta, \tag{8}$$

and

$$\tilde{H}_1(\delta) = -j \left(\frac{\hat{\alpha}}{2} \right) \frac{e^{j\frac{\delta Q}{4}}}{\sqrt{\left(\frac{\delta Q}{4} \right)^2 + \left(\frac{\hat{\alpha}}{2} \right)^2}}$$

$$\times \left\{ \sin \left[\sqrt{\left(\frac{\delta Q}{4} \right)^2 + \left(\frac{\hat{\alpha}}{2} \right)^2} \right] \right\}, \tag{9}$$

Using Eqs. (7) and (9) in Eq. (8), it is readily seen that

$$E_1(r') = A \left[-j \sin \left(\frac{\hat{\alpha}}{2} \right) \right], \tag{10}$$

as expected, and indicating a uniform output profile.

- ii. Zeroth-order output corresponding to a uniform plane wave input

Let $E_{\text{inc}}(r) = A$ so that once again $\tilde{E}_{\text{inc}}(\delta) = A(\lambda/\phi_B)\delta_k(\delta)$.

Hence, using

$$E_0(r) = \int_{-\infty}^{\infty} \tilde{E}_{\text{inc}}(\delta) H_0(\delta) e^{-j\frac{2\pi}{\lambda}\delta\phi_B r} \left(\frac{\phi_B}{\lambda} \right) d\delta \tag{11}$$

and

$$\tilde{H}_0(\delta) = -\frac{e^{-j\frac{\delta Q}{4}}}{\sqrt{\left(\frac{\delta Q}{4} \right)^2 + \left(\frac{\hat{\alpha}}{2} \right)^2}} \left\{ \sqrt{\left(\frac{\delta Q}{4} \right)^2 + \left(\frac{\hat{\alpha}}{2} \right)^2} \right.$$

$$\times \cos \left[\sqrt{\left(\frac{\delta Q}{4} \right)^2 + \left(\frac{\hat{\alpha}}{2} \right)^2} \right]$$

$$\left. + j \frac{\delta Q}{4} \sin \left[\sqrt{\left(\frac{\delta Q}{4} \right)^2 + \left(\frac{\hat{\alpha}}{2} \right)^2} \right] \right\}, \tag{12}$$

one obtains straightforwardly,

$$E_0(r) = A \frac{\phi_B}{\lambda} \frac{\lambda}{\phi_B} \left[\frac{1}{\left(\frac{\hat{\alpha}}{2} \right)} \right] \left[\frac{\hat{\alpha}}{2} \cos \left(\frac{\hat{\alpha}}{2} \right) \right] = A \cos \frac{\hat{\alpha}}{2}, \tag{13}$$

as expected, and uniform in r .

Acknowledgments

One of us (FSA) would like to express sincere appreciation for the financial support provided by the Saudi Arabia Cultural Mission. MRC would like to thank the ECE Department, University of Dayton, for providing generous travel support that enabled dissemination of this work at multiple conferences.

References

1. L. Brillouin, "Diffusion of light and x-rays by a transparent homogeneous body," *Ann. Phys.* **17**(2), 88–122 (1922).

2. C. V. Raman and N. S. Nagendra Nath, "The diffraction of light by high frequency sound waves: part I," *Proc. Indian Acad. Sci.* **2**, 406–412 (1935).
3. A. Korpel, *Acousto-Optics*, 2nd ed., Marcel Dekker, New York (1997).
4. W. R. Klein and B. D. Cook, "Unified approach to ultrasonic light diffraction," *IEEE Trans. Sonics Ultrason.* **SU-14**, 123–133 (1967).
5. S.-T. Chen and M. R. Chatterjee, "A numerical analysis and expository interpretation of the diffraction of light by ultrasonic waves in the Bragg and Raman–Nath regimes multiple scattering theory," *IEEE Trans. Educ.* **39**(1), 56–68 (1996).
6. C. Webb and J. Jones, *Handbook of Laser Technology and Applications*, 1st ed., IOP, Cornwall, UK (2004).
7. A. Korpel and T.-C. Poon, "Explicit formalism for acousto-optic multiple plane-wave scattering," *J. Opt. Soc. Am.* **70**(7), 817–820 (1980).
8. R. Pieper and A. Korpel, "Eikonal theory of strong acousto-optic interaction with curved wavefronts of sound," *J. Opt. Soc. Am. A* **2**, 1435–1445 (1985).
9. A. Korpel, C. Venzke, and D. Mehrl, "Novel algorithm for strong acousto-optic interaction: application to a phase profiled sound column," in *Proc. Ultrason. Int. 91*, Butterworth, London, pp. 111–114 (1991).
10. M. R. Chatterjee, T.-C. Poon, and D. N. Sitter Jr., "Transfer function formalism for strong acousto-optic Bragg diffraction of light beams with arbitrary profiles," *Acustica* **71**(2), 81–91 (1990).
11. M. Chatterjee and M. A. Al-Saedi, "Examination of chaotic signal encryption and recovery for secure communication using Hybrid Acousto-optic feedback," *Opt. Eng.* **50**(5), 055002 (2011).
12. M. A. Al-Saedi and M. R. Chatterjee, "Examination of the nonlinear dynamics of a chaotic acousto-optic Bragg modulator with feedback under signal encryption and decryption," *Opt. Eng.* **51**(1), 018003 (2012).
13. J. Chrostowski and C. Delisle, "Bistable piezoelectric Fabry–Perot interferometer," *Can. J. Phys.* **57**(9), 1376–1379 (1979).
14. J. Chrostowski and C. Delisle, "Bistable optical switching based on Bragg diffraction," *Opt. Commun.* **41**, 71–74 (1982).
15. L. N. Magdich and V. Y. Molchanov, "Diffraction of a divergent beam by intense acoustic waves," *Opt. Spectrosc.* **42**, 299–302 (1977).
16. L. N. Magdich and V. Y. Molchanov, "Theory of acoustooptical interaction in a high-field," *Opt. Spectrosc.* **48**, 159–161 (1980).
17. L. N. Magdich and V. Y. Molchanov, *Acoustooptical Devices and Their Applications*, Gordon and Breach, New York (1989).
18. J. Xia et al., "Image edge enhancement by Bragg diffraction," *Opt. Commun.* **128**, 1–7 (1996).
19. P. P. Banerjee, D. Cao, and T.-C. Poon, "Basic image processing operations using acousto-optics," *Appl. Opt.* **36**, 3086–3089 (1997).
20. J. Durmin, J. J. Miceli, and J. Eberly, "Diffraction-free beams," *Phys. Rev. Lett.* **58**, 1449–1501 (1987).
21. Z. Bouchal, "Nondiffracting optical beams: physical properties, experiments, and applications," *Czech. J. Phys.* **53**(7), 537–624 (2003).

Monish R. Chatterjee received the MS and PhD degrees in ECE from the University of Iowa in 1981 and 1985, respectively. Since 2002, he has been a professor at the University of Dayton. He has authored over 60 papers in archival journals and conference proceedings, several book chapters, three literary books, numerous literary essays, and presented over 100 papers at international conferences. He is a senior member of the IEEE and the OSA, and a member of SPIE and Sigma Xi.

Fares S. Almejadi received his BSEE degree in electrical engineering from Umm Al-Qura University, Makkah, Saudi Arabia, in 2009, and the MSEE degree from the University of Dayton, in 2011. Currently, he is completing his research for the PhD degree at the University of Dayton, Dayton, Ohio. His areas of research interests include acousto-optic interactions, nonlinear optics, signal processing, and digital communications. His doctoral work has resulted in two conference presentations and proceedings articles.